Fatigue Behavior of Nodular Cast Iron after Gas Nitriding

R. Konečná[1, a], G. Nicoletto[2, b], V. Konstantová[3] and P. Jančovič[1]

[1]Dept. of Materials Engineering, University of Žilina, Žilina, Slovakia

[2]Dept. of Industrial Engineering, University of Parma, Parma, Italy

[3]Dept. of Design and Machine Elements, University of Žilina, Žilina, Slovakia

[a]radomila.konecna@fstroj.uniza.sk, [b]gianni.nicoletto@unipr.it

Keywords: Nodular cast iron, nitriding, fatigue test, structure, defects, Murakami statistical method, fracture surface.

Abstract. The paper presents and discusses the structural characterization, the fatigue behavior and the fracture mechanisms of gas nitrided nodular cast irons (NCIs). Fatigue behavior is strongly dependent on structure but also on defects and inhomogeneity. Results of fatigue behavior on nitrided NCIs show a significant increase in fatigue limit and a different trend in the S/N curve in dependence of type matrix. A link between microstructure and fracture mechanisms is found in factors such as structure of NCIs, content of carbides, penetration depth and concentration of nitrogen on the boundaries of ferritic grains below the white layer. The Murakami's statistical largest size description of casting defects (pores) and inhomogeneities (nodules) is proposed and assessed using the present fatigue data.

Introduction

Nodular cast irons (NCIs) combine the cost-effective casting technology with high fatigue strength [1] and it can be produced according to the classical or synthetic casting procedure, which is more economical because steel scrap is added to the charge instead of a part of pig iron [2]. Until recently ferrosilicon (FeSi) has been mainly used as an additive to the liquid metal to increase the Si content and to obtain approximately eutectic composition. In the present time, however, silicon carbide (SiC) is predominately used as addition because it increases not only the content of silicon but also the content of carbon [2, 3]. For fatigue-critical application, the population of defects created in the casting process and the graphite nodule characteristics influence NCIs fatigue behavior. Typically, fatigue endurance is reduced when the size of porosity increases. Therefore, the quality of the castings is related to the porosity control.

The surface characteristics of NCIs may be modified for fatigue-critical applications by thermo-chemical surface treatments, such as nitriding. When a part is exposed to a nitriding medium, nitrogen will diffuse into the metal for a controllable depth forming an outside layer called white layer (i.e. thickness generally ranges between zero and 25 μm) and subsurface diffusion and subdiffusion zones [4].

The present work is aimed to identify the influence of different structural factors on fatigue lifetime of nitrided NCIs. Light microscopy was performed to analyze the microstructure and pores in the material after fatigue testing. The statistical method proposed by Murakami [5], based on the largest extreme value determination (LEVD) was used to evaluate the porosity size population. Fracture surfaces were selected to determine places of crack initiation and the fracture micromechanisms of nitrided specimens.

Material and experimental methodology

Experimental materials were: i) the classical melt of nodular cast iron (denominated melt B) with fully ferritic matrix, and ii) 2 synthetic melts of NCI (denominated melt C and T) where as additive material silicon carbide (SiC) was added into the liquid metal to obtain $S_C \sim 1$ and a high content of effective ferrite (EF). The chemical composition of melts was comparable with approximately eutectic composition.

Fatigue specimens were extracted from different real castings in the case of melt B and from melted bars of melt C and T. Two sets of smooth fatigue specimens with 6-mm-dia were prepared by machining. Then, one set of specimens of each material was subjected to a nitriding treatment. A Nitreg® patented controlled potential process was used on specimens of melt B and an optimized gas nitriding treatment on specimens of melts C and T. In case of melt T the fatigue behavior of untreated material was not studied because of structure similarity with melt C. The fatigue data for untreated and nitrided specimens were obtained on a rotating-bending testing machine operating at 50 Hz (i.e. load ratio R = -1). The fatigue limit σ_{oc} was determined according to a reduced staircase method [6] for melt B. For melts C only two stress amplitude levels were investigated to assess the trend of S/N curves for untreated or nitrided specimens. Different stress amplitude levels were applied on nitrided specimens of melt T to investigate the S/N curves trend.

The structural analysis was performed on polished and etched specimen cross sections of specimens after fatigue testing (melt B) and cast bars of synthetic melts with the light metallographic microscope according to the standard EN STN 42 0461 and according to the methods of quantitative metallography. The nitrided layer was analyzed on cross sections of fatigue specimens after testing using color etching to reveal their composition. The image analysis program LUCIA Metallo 5.0 was applied to extensive and detailed measurement of porosity on no etched metallographic sections. To characterize pore size the LEVD theory proposed by Murakami [5] was used.

The fatigue fracture surfaces were investigated in SEM on selected nitrided specimens tested at the same stress level and showing different fatigue lives to identify possible origin of fatigue crack initiation.

Results and discussion

Structural characterization. The structure of melt B represents fully ferritic NCI with a regular distribution of graphite nodules with size ranging from 15 to 60 μm (VI 6, 7), see Fig. 1a. Using EDAX analysis in case of specimens B3 and B4 carbides especially with Ti, Cr and V were found in the matrix, Fig. 1b. A discontinuous network of carbides (more visible in case of specimen B4) with the presence of microshrinkages on the boundaries of eutectic cells was observed.

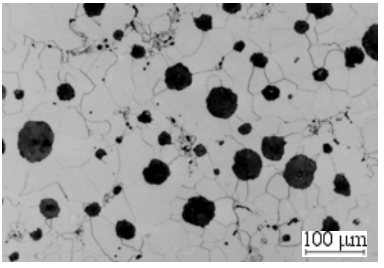

a) fully ferritic, EF = 86 %

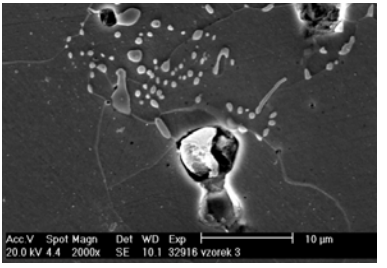

b) carbides, SEM

Fig. 1 Microstructure of melt B, etched with 3 % nitric acid

The structure of specimens taken from synthetic melts C and melt T showed a similarity in case of EF (content of ferrite in the volume of specimen) content. The structure of NCIs can be divided in 3 groups according to EF: i) almost fully ferritic (EF from 86 to 70 %), ii) ferritic-pearlitic (EF from 69 to 52 %), and iii) pearlitic-ferritic (EF from 51 to 41 %), Fig. 2. The graphite nodules were observed in fully or not fully globular shape predominately with size ranging from 30 to 60 μm (VI 6) and with a small ratio of size ranging from 60 to 120 μm (VI 5).

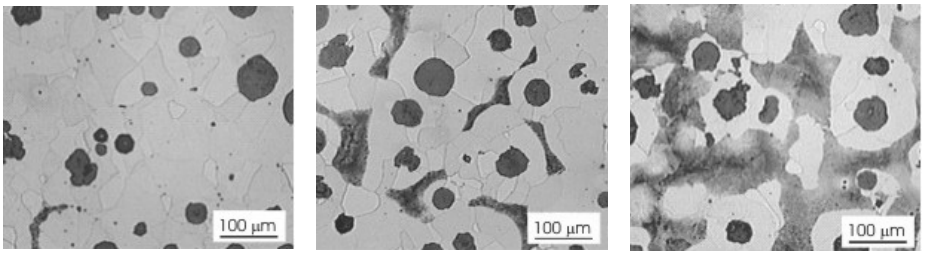

a) almost ferritic b) ferritic-pearlitic c) pearlitic-ferritic

Fig. 2 Characteristic microstructures of synthetic melt C and T of NCIs, etched with 3 % nitric acid

A nitrided layer is formed by a thin white layer (WL) on the surface of specimens, diffusion zone (DZ) and subdiffusion zone (SDZ), Fig. 3a. The WL was mostly continuous with variable thickness from 10 to 28 μm for melt B, respectively from 9 to 33 μm for melt C, and for melt T from 5 to 25 μm in the dependence of the presence of graphite near the surface of specimen.

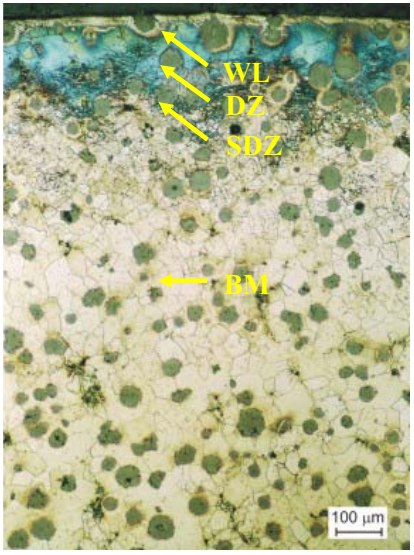

a) zones in nitrided layer, etched by 5 % molybdenum acid

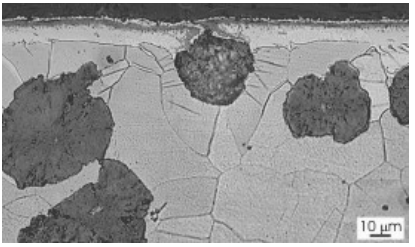

b) WL and carbonitride layer, etched by 3 % nitric acid

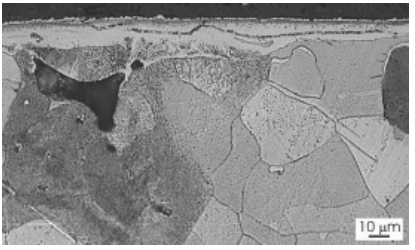

c) crack in WL and microshrinkage in pearlite etched by 3 % nitric acid

Fig. 3 Structural characteristics of nitrided layer of nodular cast iron

In all specimens a thin dark layer, which is most probably a carbonitrided layer (because of high content of carbon in NCI) in WL was identified, when a high magnification was used, Fig. 3b. Polyedric ferritic grains in DZ were observed, Fig. 3. When structure was etched with Klemm I the nitrides could be observed on the boundaries of ferritic grains in DZ as white places. In special cases it was found that graphite particles on the surface of specimen were not covered by WL, Fig. 3 a, b, small cracks in WL were observed, an example see Fig. 3c or microshrinkages just below WL in pearlitic area were found, see Fig 3c. These inhomogeneities in nitrided layer show a worse quality of nitrided layer which can in the fatigue testing influence the fatigue life of tested specimens.

Fatigue properties. The fatigue data obtained on the different melts and in the as-cast and after nitriding are now presented. In all cases the nitriding treatment is demonstrated to give a very significant improvement of the fatigue response, comparable or higher of that observed in steels. The increase in the fatigue strength associated to the nitriding treatment is due to the simultaneous formation of the hardened surface layer and of favorable compressive residual stresses. The S/N curves of the untreated and nitrided melt B are shown in Fig 4. The fatigue limit is σ_{oc} = 169 MPa for untreated and σ_{oc} = 381 MPa for nitrided NCI of melt B. The S/N data of the nitrided NCI are fitted with two parallel lines because specimens subjected to the same applied stress amplitude showed fatigue lives differing by more than two orders of magnitude, an indication of different initiation mechanisms described elsewhere, [7].

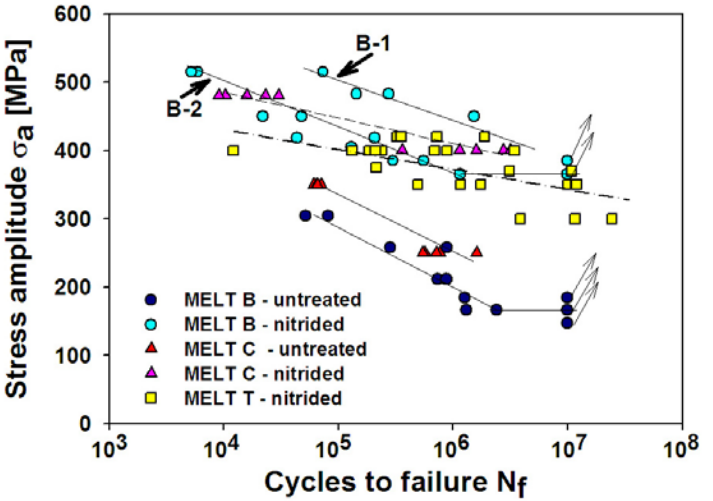

Fig. 4 Fatigue data

The data and the trend of S/N curves of melt C, Fig 4, showed higher number of cycles to failure for the same applied stress amplitude for untreated melt C because of the lower EF content compared to the melt B. The fatigue data of untreated and nitrided specimens of melt C showed no significant dependence of number of cycles to the failure on content of EF within individual specimens. The fatigue data of melt T were obtained only for the nitrided conditions and are quite scattered about the mean S/N curve shown in Fig 4.

Concerning the influence of the matrix on the fatigue behavior, the reduction of the effective ferrite in the matrix tends to increase the fatigue resistance for NCI in the untreated condition. This increase is not maintained after nitriding. All nitrided data appear to distribute within a single, wide, scatter band, although a difference in response among the three NCIs appears in terms of the slope

of the S/N curves. This could be an indication that different micromechanisms are operative in the pearlite and ferrite after nitriding. This point, however, needs further verification.

LEVD application. An extensive investigation was performed to find the influence of different structural factors on fatigue lifetime of NCI in the nitrided condition. The most important factors influencing fatigue life are size and shape of casting defects (microshrinkages) and graphite particles, the number of graphite particles per mm^{-2} N and content of EF. Since EF and N did not play a very evident role in the data of Fig. 4, defect type and content (i.e. graphite nodules vs. microshrinkages as potential initiator sites of fatigue cracks) in the matrix were investigated. The Murakami LEVD method [5] was applied to characterize the severity of nodules and microshrinkages for fatigue behavior. Sets of largest defects found using a microscope were determined, sorted and plotted in the probability plot of Fig. 5, where the function

$$y_j = f(\sqrt{area_{\max,j}}) \tag{1}$$

shows a linear trend.

The largest defect size distribution was evaluated on specimens of each melt tested at the same stress amplitude level and with a very different fatigue life. The specimen B3 with long fatigue life is characterized by smaller pore sizes, than the specimen B4 with short N_f, see Fig. 5a. The graphite nodules size dependence in the Fig. 5a shows not big difference between both specimens. However, if the distributions are extrapolated to some representative cross-section area, it is concluded that graphite nodules are critical for B3 (red dot) and pores are critical for B4 (green dot).

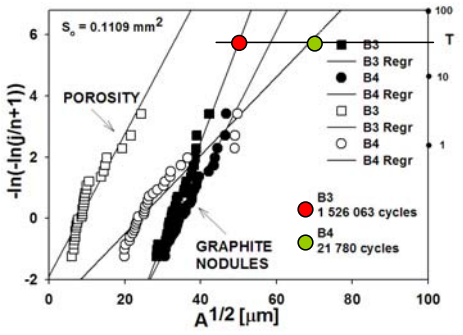

a) melt B

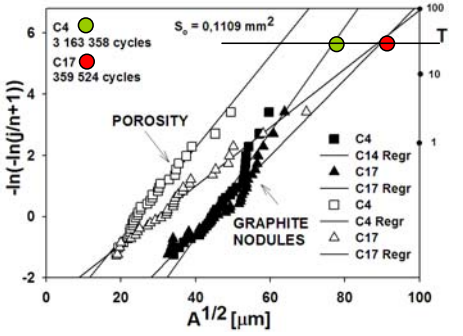

b) melt C

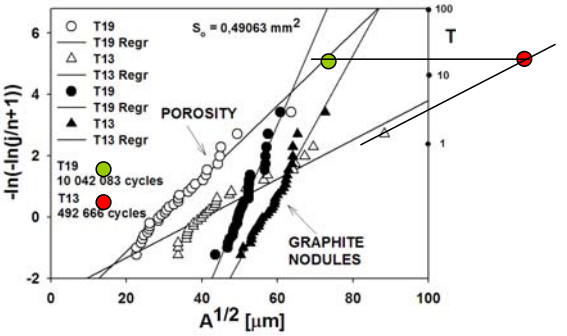

c) melt T

Fig. 5 Defect size dependence of selected specimens

A correlation between defect sizes and fatigue lives can be applied to the synthetic C and T melts. Specimens C4, C17 and T19, T13 present results of two specimens from each group tested at the same stress amplitude. The specimen C4 with high fatigue life (N_f = 3 163 358) is characterized by small pore size compared to the specimen C17 with low fatigue life (N_f = 359 524), see Fig. 5b and the similar result were found for specimen T19 (smaller pore size) and T13 with low fatigue life, Fig. 5c. In these cases, graphite nodules are critical for specimen C4 and casting pores are critical for C17 while both T13 and T19 are mainly affected by casting pores.

Fractographic analysis. Fatigue fracture analysis was performed always on 2 specimens tested at the same stress amplitude but with greatly different number of cycles to the failure for each melt. In all fatigue fracture surfaces of untreated and nitrided specimens of analyzed NCIs, two regions were found: i) the fatigue region – light, and ii) the region of final static failure – dark, see Fig. 6.

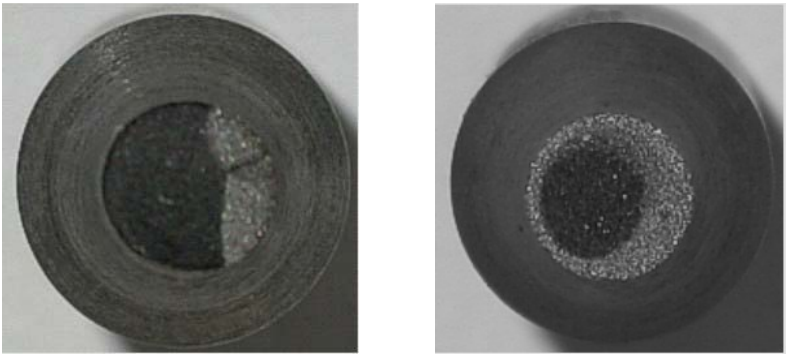

a) untreated b) nitrided

Fig. 6 Macrograph of fatigue fracture surface of NCI, SEM

Stable propagation of fatigue cracks occurs in the light region, while the dark corresponds to unstable crack propagation to the fracture. A macrograph shows that the fatigue region is situated differently in the dependence of treatment. In case of nitrided specimens the fatigue region can be observed on peripheral area of fracture surface, see Fig. 6b and it was found that the extent of the fatigue areas increased with decreasing of stress amplitudes.

Multiple initiations of fatigue crack were associated to the presence of radial stairs, example see Fig. 7a, on the fracture surface of both (classical and synthetic) melt of NCIs in untreated and nitrided conditions. It was very complicated to identify a place of crack initiation because the cracks can initiate from different places: i) microshrinkages near the surface of specimen or after nitirding below the white layer, Fig. 7b, ii) interface of the graphite particles/matrix (ferrite or WL), and iii) small microcracks in the white layer when the nitrided layer is too hard.

After initiation, fatigue cracks propagated in two directions: propagation through the WL to the surface of specimen was characterized by transcrystalline cleavage and into the material (from micro shrinkage below the WL), see Fig. 7b, and was characterized by different fracture micro mechanism depending on the places of crack propagation. In DZ and SDZ cracks propagated by intercrystalline cleavage along grain boundaries of ferrite grains, where high content of N was found, Fig. 7c,d and then by formation of fine striations with multiple localities in sub-diffusion zone. The presence of striations, Fig. 7e, confirmed the plastic deformation in the ferrite. Fatigue cracks propagated mainly through ferrite grains by transcrystalline cleavage. In SDZ of the specimens of melt C or T, where a limited content of pearlite was observed and formed small localities in ferritic matrix, the formation of fine dimples initiated on inclusions in pearlite were observed.

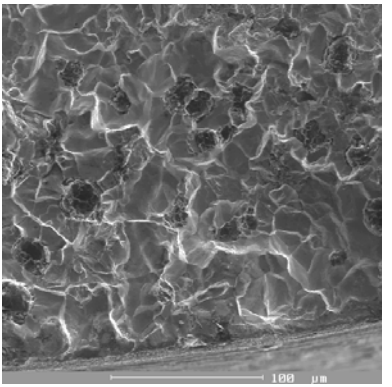

a) radial stairs, untreated specimen

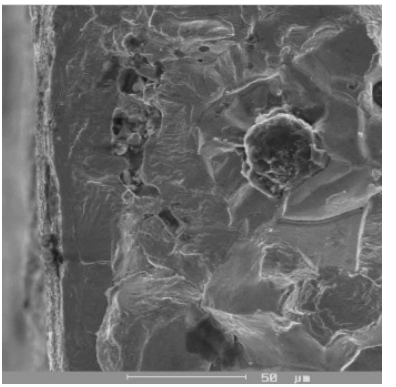

b) microshrinkage, nitrided specimen

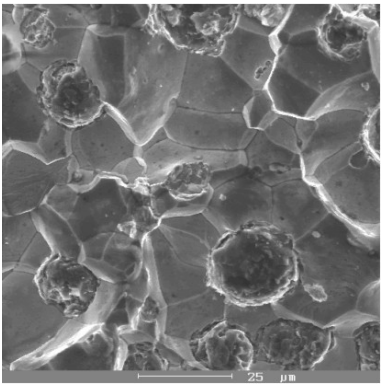

c) intercrystaline decohesion DZ

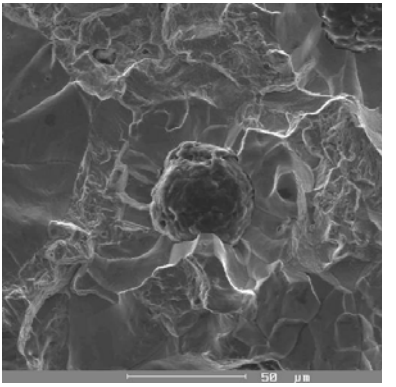

d) SDZ

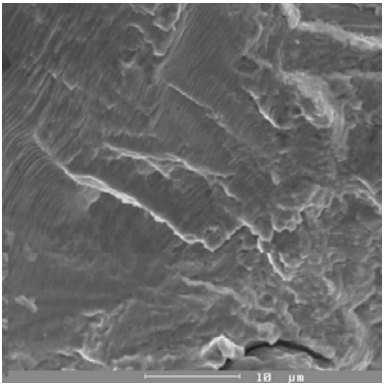

e) striation

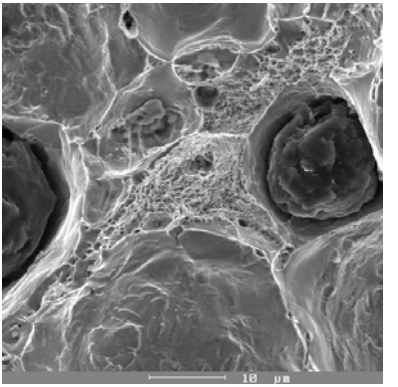

f) final fracture surface

Fig. 8 Fatigue fracture surface, SEM

In the region of final static fracture of untreated and nitrided specimens of analyzed NCIs, cracks propagated by transcrystalline ductile fracture of ferrite with dimple morphology, Fig. 7f. Fine dimples in ferrite are initiated on carbides in the case of melt B. Transcrystalline ductile fracture of pearlite with fine dimples was found in the case of melt C and T with a limited content of pearlite in

the matrix, see Fig. 7f. In the case of low effective ferrite content in synthetic melts the transcrystalline continuous cleavage of pearlite with rivers was observed.

Summary

The paper presented the structural characterization, the fatigue behavior and the study of the fatigue fracture mechanisms of gas nitrided nodular cast irons (NCIs). The following main conclusions are reached:

- The content of effective ferrite and number of graphite particles do not show direct influence on fatigue behavior in the nitrided NCIs.
- Fatigue cracks could initiate from defects i.e. graphite particles on surface, microshrinkage near the surface or below the white layer.
- Largest pore and graphite nodule sizes were characterized using Murakami approach based on the LEVD theory.
- A reasonable correlation between largest defect (graphite nodule or pore) size and fatigue lifetimes for different specimens tested at the same stress level was found.

Acknowledgments

This work was done as a part of the SK/IT project No10/NT and a part of SK/CZ project No SK36/CZ 37 and of VEGA grant No.1/3194/06. It is also consistent with the objectives of MATMEC, an Emilia-Romagna regional net-lab (http://www.matmec.it/).

References

[1] DAVIS, J. *Cast Irons/Metallurgy and Properties of Ductile Cast Irons.* USA: ASM Specialty Handbook, The Materials Information Society, 1996.

[2] KARSAY, S. I. *Tvárna liatina I. Výroba*. 1. vyd. Trenčín : Fompex, 1996.

[3] KONEČNÁ, R., ZÁHOROVÁ, B. and MATEJKA, M. Vplyv prísady SiC na porušovanie tvárnej liatiny. *Materiálové inžinierstvo*, 2000, roč. 7, č. 4, s. 27-34.

[4] SINHA, A. *Physical metallurgy handbook*. NY: McGraw-Hill, 2003.

[5] MURAKAMI, Y.: *Metal fatigue: Effect of Small Defects and Nonmetalic Inclusions*. First edition, ELSEVIER: 2002.

[6] BOKŮVKA, O., NICOLETTO, G., KUNZ, L., PALČEK, P. and CHALUPOVÁ, M.: *Low & High Frequency Fatigue Testing*. CETRA, Žilina, EDIS 2002.

[7] KONEČNÁ, R., MAJEROVÁ, V., NICOLETTO, G. and OMELKA, A. Influence of Matrix Structure on the Fatigue Response of Nitrided Nodular Cast Iron. In Zborník z konferencie 21. Dny tepelného zpracování, Jihlava, 2006, pp. 89-97.